Raman spectra and improper ferroelastic phase transition in $LiNH_4SO_4$ single crystal

1999 J. Phys.: Condens. Matter 11 889

(http://iopscience.iop.org/0953-8984/11/3/027)

J. Phys.: Condens. Matter **11** (1999) 889–903. Printed in the UK PII: S0953-8984(99)97634-8

Raman spectra and improper ferroelastic phase transition in $LiNH_4SO_4$ single crystal*

Yu I Yuzyuk†‡, V I Torgashev†, I Gregora‡ and A H Fuith§

† Faculty of Physics, Rostov State University, Zorge 5, 344090, Rostov-on-Don, Russia
‡ Institute of Physics, Academy of Sciences of the Czech Republic, Na Slovance 2, 182 21 Prague 8, Czech Republic
§ Institut für Experimentalphysik, Universität Wien, Strudlhofgasse 4, A-1090 Vienna, Austria

Received 16 September 1998, in final form 29 October 1998

Abstract. Polarized Raman spectra of lithium ammonium sulphate (LAS) single crystals in the temperature range 40–290 K have been studied and compared with the available data. Careful analysis of their temperature evolution it made possible to propose a comprehensive assignment of the observed Raman active phonon modes and to gain deeper insight into the lattice dynamics of this crystal in the low-temperature ferroelastic phase III. In particular, numerous new modes connected with doubling of the unit cell were unambiguously identified in agreement with group-theoretical predictions. The peculiar temperature evolution of the spectra below the II $\rightarrow$ III transition temperature T_2 (284 K) is explained by coexistence of both phases, with metastable polar clusters and heterophase fluctuations persisting in a wide temperature range below T_2. This interpretation accounts also for other anomalies observed in macroscopic properties of LAS in this temperature interval.

1. Introduction

The beta form of lithium ammonium sulphate, β-$LiNH_4SO_4$ (hereafter denoted LAS), is a weak ferroelectric at room temperature. At atmospheric pressure LAS exhibits the following sequence of phase transitions (PTs) [1–3]

$$\begin{array}{ccccccc} D_{2h}^{16}(v) & & C_{2v}^{9}(v) & & C_{2h}^{5}(2v) & & C_{s}^{4}(4v) \\ & T_1 = 460\ \text{K} & & T_2 = 284\ \text{K} & & T_3 = 27\ \text{K} & \\ Pnma & & Pn2_1a & & P12_1/a1 & & \text{Cc} \\ \text{phase I} & & \text{phase II} & & \text{phase III} & & \text{phase IV,} \end{array}$$

where v denotes the primitive cell volume of the orthorhombic phase I ($Z = 4$) and T_i denotes the PT temperatures. There is at least one more phase (C_2^2) stable above 700 MPa. The crystal structure of LAS, closely related to that of tridymite SiO_2, has been determined in all phases [3-7].

A thermodynamic theory taking into account two coupled order parameters and describing the sequence of PTs in LAS (not including phase IV which was discovered later on) was developed [8]. According to this theory the first PT (at $T_1 = 460$ K) was classified as a pseudoproper ferroelectric induced by an order parameter of B_{2u} symmetry which is bilinearly coupled to the P_y polarization component of the same symmetry. The ferroelastic PT at $T_2 = 284$ K is associated with doubling of the orthorhombic unit cell along the a-axis. Since

* Dedicated to the late F Smutný.

0953-8984/99/030889+15$19.50

the phase III is not a subgroup of phase II, the I–III PT has been considered and it has been shown that this symmetry transformation can be induced by a second two-component order parameter transforming according to an irreducible representation at the X point ($\boldsymbol{k} = \frac{1}{2}\boldsymbol{a}^*$) of the Brillouin zone ($\tau_2(\boldsymbol{k}_{21})$ in the notation introduced by Kovalev [9]). The form of the phase diagram was derived and compared with that constructed on the basis of published experimental data.

Experimental Raman studies of LAS are numerous, most of them being devoted to detailed assignment of LO–TO components in the room-temperature polar phase [10], to the high-temperature ferroelectric transition [11–13] or to the high-pressure transition [14]. However, lattice dynamics in the low-temperature ferroelastic phase of LAS has not been sufficiently well studied and there are only very few papers where some fragmental Raman spectra restricted to the frequency region of external modes were reported [12, 15, 16]. Unfortunately, the first Raman measurements revealing a soft mode [15] were performed in the temperature range 183–295 K and the symmetry classification was based on the assumption that the symmetry of phase III is C_2^2. Unpolarized Raman spectra on a crystalline powdered sample at temperatures between 10 and 300 K in the 10–500 cm^{-1} frequency range [16] allowed just to confirm the occurrence of a low-temperature PT: the spectra at 10 K showed a tremendous increase in the number of narrow bands.

The low-temperature properties of LAS have not been sufficiently studied to date and numerous discrepancies were found in the published data. The two-phase state in LAS below the II $\rightarrow$ III first-order PT has already been reported [1], where direct observations during very slow cooling revealed supercooling of the phase II by as much as several tens of degrees, accompanied by gradual growth of regions of the phase III. The spontaneous polarization drops to zero at the II $\rightarrow$ III PT and exhibits small thermal hysteresis of a few degrees; nevertheless the dielectric hysteresis loops were observed on cooling–heating runs below T_2 in LAS and its deuterated analogue [23]. The existence of a two-phase system is also sufficient to explain the piezoelectric effect [1] below T_2, weak dielectric anomalies at 258 K and 160 K and the pyroelectric response [20] observed down to 215 K. Finally, the additional anomaly of the (molar) heat capacity observed at 248.1 K from DSC measurements [16] is more likely due to supercooling of the phase II since the anomaly vanishes after six or seven thermal cycles between 300 and 150 K. Finally, two PTs proposed from PMR (proton magnetic resonance) measurements at 133 and 81 K [18, 19] were not confirmed by dielectric measurements [17] or by any other method and direct x-ray measurements have not revealed any structural transformation down to 27 K [3].

The present contribution reports detailed assignments of Raman active modes and their temperature evolution in the phase III observed in the temperature range 290–40 K. The vibrational spectra are discussed in correlation to the reported Raman measurements in the paraelectric phase I performed at 473 K [21].

2. Experimental details

Polarized Raman spectra have been measured on samples in the form of carefully oriented and optically polished rectangular parallelepipeds $4 \times 2 \times 1$ mm^3 with edges x, y, z parallel to the orthorhombic crystallographic axes $\boldsymbol{a}$, $\boldsymbol{b}$, $\boldsymbol{c}$, respectively [12]. The sample was placed in a continuous-flow cryostat (Leybold VSK 4-300) where it was convection cooled in He exchange gas. The temperature was measured by a chromel–constantan thermocouple attached to the sample holder. The actual sample temperatures were estimated to differ by less than 1 K from the temperature readings. The 488 nm Ar^+ laser line at 500 mW was used for excitation in the right-angle scattering geometry. The scattered light was analysed using a PC-controlled

double-grating spectrometer (Spex-14018) equipped with a standard single-channel photon counting detector. The spectral slit width was set to 1 or 2 cm^{-1} (below and above 1200 cm^{-1}, respectively).

3. Symmetry classification of phonon modes

According to x-ray data all the Li^+, NH_4^+ and SO_4^{2-} ions occupy fourfold sites on the mirror plane of C_s symmetry in the paraelectric phase (I), whereas in the ferroelectric phase II and ferroelastic phase III they occupy fourfold sites of C_1 symmetry. As follows from the factor-group analysis [12], the dynamics of the crystal lattice is described in terms of 132 phonon modes in phases I, II and 264 modes in phase III:

phase I $(20A_g + 13A_u + 13B_{1g} + 19B_{1u} + 20B_{2g} + 12B_{2u} + 13B_{3g} + 19B_{3u})_{vib}$
$+ (B_{1u} + B_{2u} + B_{3u})_{ac}$

phase II $(32A_1 + 33A_2 + 32B_1 + 32B_2)_{vib} + (A_1 + B_1 + B_2)_{ac}$

phase III $(66A_g + 65A_u + 66B_g + 64B_u)_{vib} + (A_u + 2B_u)_{ac}$

where subscript vib denotes IR and/or Raman active optical vibrations and ac denotes the acoustic phonons.

Since there is no group–subgroup relation at the II–III transition, vibrational spectra of LAS in phase III are formed from the modes of the Γ and X points of the Brillouin zone of phase I at the I–III antiferrodistortive PT due to unit cell doubling at this hypothetical transition. Internal vibrations of tetrahedral sulphate and ammonium groups are rather well separated and one can make their detailed assignment. Out of the total number of modes, 72 (in phase I and II) and 144 (in phase III) are internal vibration modes of sulphate and ammonium ions, three are zero-frequency acoustic modes and the remaining ones are external (librational and translational) optical modes.

The fundamental internal vibrations of NH_4^+ and SO_4^{2-} ions allowed under the T_d point group consist of one nondegenerate fully symmetric stretching $\nu_1(A_1)$, one doubly degenerate bending ν_2 (E), one triply degenerate asymmetric stretching ν_3 (F_2) and one triply degenerate bending ν_4 (F_2). The fundamental modes of the NH_4^+ and SO_4^{2-} ions have been labelled by superscripts N and S, respectively.

Correlation diagrams representing formation of the vibrational spectra for internal modes of tetrahedral ions of LAS in phases I and III are presented in table 1.

4. Experimental results and discussion

As expected from the selection rules for monoclinic phase III, abrupt changes in the Raman spectra were observed below T_2: new lines appear due to the phonon branch folding and A_g lines become active for the α_{xz} component of the Raman tensor (the two-fold axis in phase III is parallel to the y-axis). Because of the low site symmetry of all crystal units in phase III, Raman spectra of α_{xx}, α_{yy}, α_{zz} and α_{xz} contain equivalent information. Nevertheless, by examining spectra for all crystal orientations one can obtain detailed information about peculiarities of the crystal structure. The Raman spectra of LAS at 40 K for different scattering geometries are shown in figure 1; the corresponding frequencies and their assignments are listed in table 2.

4.1. Internal modes of SO_4^{2-}

The fully symmetric stretching vibration ν_1^S (free ion value 983 cm^{-1}) was observed at 1005 cm^{-1} in both A_g and B_{2g} symmetry species in the high-temperature phase I [21].

Table 1. Correlation diagram for internal vibrations of SO_4^{2-} and NH_4^+ tetrahedral ions in LAS.

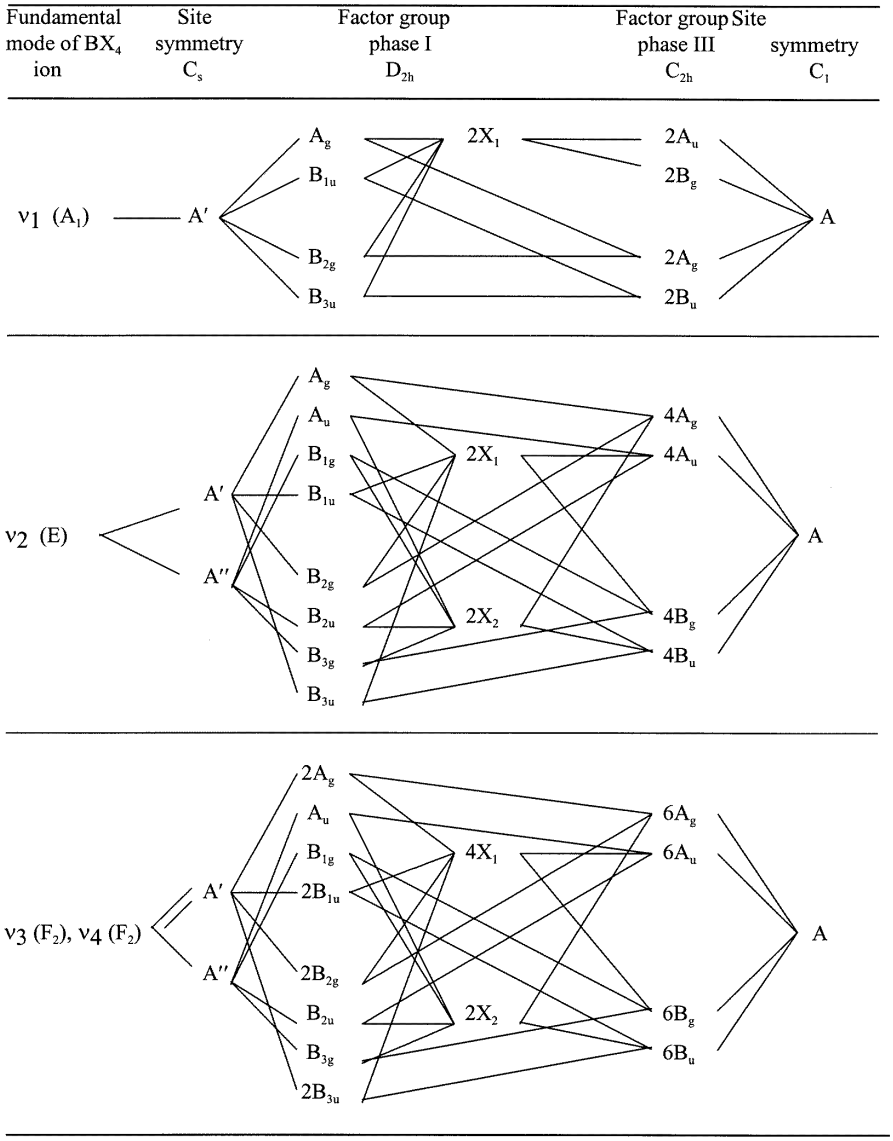

In accordance with the factor-group analysis, a well defined doublet at 1006–1017 cm^{-1} was observed in phase III in all diagonal orientations and its intensity in the $Y(XZ)X$ geometry increased abruptly below T_2. A doublet at 1006–1017 cm^{-1}, corresponding to ν_1^S in the B_g species, was found also at 40 K. As follows from the correlation diagram (table 1), this doublet originates from the edge of the Brillouin zone (irreducible representation X_1) which accounts for its rather low intensity just below T_2. The intensity increases on cooling and, as reported in figure 2, the doublet becomes well resolved below 120 K only.

Among the four A_g and four B_g components expected for the doubly degenerate ν_2^S bending mode (free ion value 450 cm^{-1}) in phase III, two pairs—$2A_g$ (474, 484 cm^{-1}) and

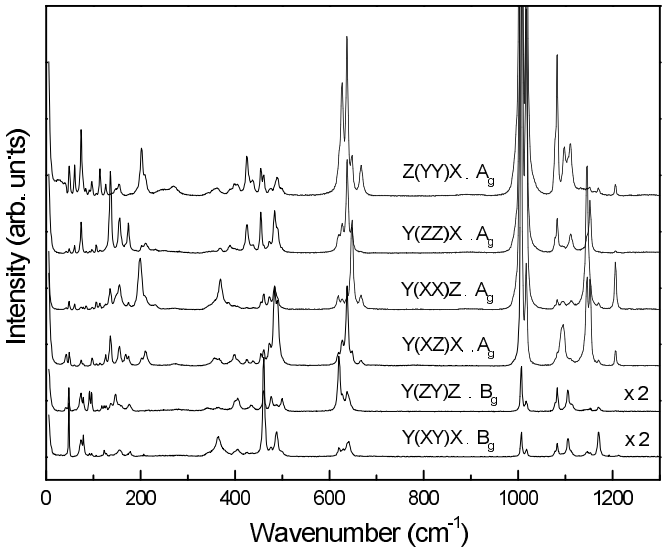

(*a*)

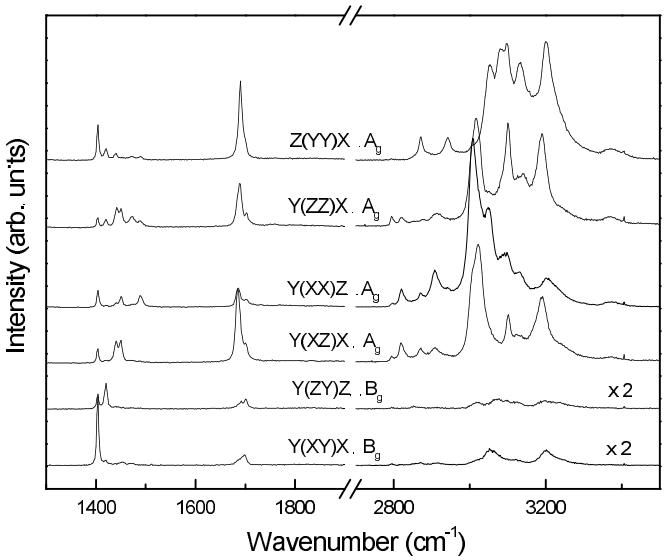

(*b*)

Figure 1. Overall Raman spectra of LAS at 40 K for six scattering geometries: (*a*) external vibrations and internal vibrations of SO_4^{2-} ions; (*b*) internal vibrations of NH_4^+ ions.

$2B_g$ (476, 484 cm^{-1})—originate from the zone centre $2A_g + 2B_{2g}$ modes of phase I, while the other two come from X_1 and X_2 phonons correlated with $2A_g + 2B_g$. The latter were found unambiguously at 490 and 500 cm^{-1} in A_g spectra and at 489 and 498 cm^{-1} in B_g spectra at 40 K.

In the region of the triply degenerate ν_3^S asymmetric stretching mode (free ion value 1105 cm^{-1}) six A_g and six B_g lines are expected in phase III. Four A_g components originate from $2A_g + 2B_{2g}$ zone-centre modes of phase I, and two come from the zone-edge modes.

Table 2. Frequencies (in cm^{-1}) of the observed Raman lines in LAS single crystal at 40 K.

Frequencies and species			Assignment	Frequencies and species				Assignment	Frequencies and species				Assignment
42	A_g		External	474	A_g				1403	A_g	B_g		
49	A_g	B_g	modes	476		B_g			1418		B_g		
60	A_g			484	A_g				1420	A_g			
62		B_g		489		B_g	ν_2^S		1440	A_g		ν_4^N	
74	A_g	B_g		490	A_g				1443		B_g		
79	A_g	B_g		498		B_g			1450	A_g			
85	A_g			500	A_g				1454		B_g		
93		B_g							1473	A_g	B_g		
97	A_g	B_g		620	A_g	B_g			1490	A_g			
107	A_g	B_g		628	A_g								
114	A_g			630		B_g			1686	A_g	B_g		
118		B_g		637	A_g		ν_4^S		1690	A_g	B_g	ν_2^N	
123		B_g		638		B_g			1698	A_g	B_g		
127	A_g	B_g		641		B_g			1702	A_g	B_g		
137	A_g	B_g		648	A_g								
148	A_g	B_g		667	A_g				2794	A_g			
155	A_g	B_g							2821	A_g			
169	A_g			1006	A_g	B_g	ν_1^S		2871	A_g			
175	A_g	B_g		1017	A_g	B_g			2880	A_g		$2\nu_4^N$	
179		B_g							2911	A_g			
202	A_g			1078	A_g	B_g			2940	A_g			
210	A_g			1083	A_g	B_g							
230	A_g			1090	A_g				3006	A_g			
270	A_g			1096	A_g		ν_3^S		3022	A_g	B_g		
280		B_g		1105		B_g			3048	A_g		ν_1^N	
342	A_g	B_g		1112	A_g	B_g			3054	A_g	B_g		
356	A_g			1146	A_g	B_g			3072		B_g		
365	A_g	B_g		1152	A_g	B_g			3080	A_g		$\nu_2^N + \nu_4^N$	
369	A_g			1170	A_g	B_g			3100	A_g	B_g		
376		B_g		1206	A_g		N–H $\cdots$ O		3125		B_g		
390	A_g						bending		3133	A_g		ν_3^N	
400	A_g	B_g							3140	A_g			
406	A_g	B_g							3190	A_g			
425	A_g	B_g							3196		B_g	N–H $\cdots$ O	
435		B_g							3200	A_g	B_g	stretching	
439	A_g								3215	A_g			
455	A_g								3225		B_g		
461	A_g	B_g							3240	A_g	B_g	$2\nu_2^N$	
									3380	A_g			

In contrast only two B_g lines originate from zone-centre modes (B_{1g} + B_{3g}) of phase I, while four of them arise due to the zone folding. However, the number of lines observed in the region 1050–1250 cm^{-1}, where corresponding components are expected, considerably exceeds that 'allowed' by factor-group analysis: nine A_g and seven B_g lines were unambiguously observed at 40 K. The existence of additional lines in this spectral range may be an evidence for the presence of the hydrogen bonding: the well separated and polarized line at 1206 cm^{-1} may be attributed to N–H $\cdots$ O in-plane bending modes. The corresponding out-of-plane bending mode should be located at lower frequencies and its identification is impossible because of interaction with the ν_3^S mode. The temperature evolution of the line at 1206 cm^{-1} speaks

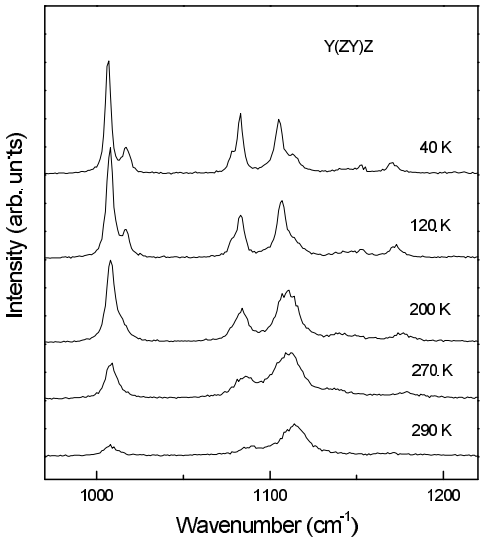

Figure 2. Temperature evolution of the stretching ν_1^S and ν_3^S internal modes in LAS observed for $Y(ZY)Z$ scattering geometry.

in favour of the proposed assignment. Namely, at the II–III transition this line disappears in $Y(ZZ)X$ geometry and appears as a weak line in $Y(XX)Z$, where on further cooling down to 40 K its intensity increases considerably (see figure 3). This fact may be connected with the partner of the H1 atom changing from O(iii′) to O(iv) through the II–III structural transformation. Corresponding changes in the hydrogen bond orientations have been indeed observed in x-ray measurements [7]. Since the site symmetry of the sulphate ions is C_1 in both phases, such behaviour could not be expected for one of the ν_3^S mode components at the II–III PT. These arguments disqualify possible attribution of the 1206 cm^{-1} line to an overtone ($2\nu_4^S$) or a summation band ($\nu_4^S + \nu_2^S$). Also, the line is rather narrow and strong for a second-order feature: our spectra show only very weak signatures of the $2\nu_2^S$ and $2\nu_1^S$ overtones near 880 cm^{-1} and 2020 cm^{-1}, respectively.

The last fundamental triply degenerate bending vibration ν_4^S (free ion value 611 cm^{-1}) should have six A_g and six B_g lines originating in the same manner as the components of the ν_3^S mode. In fact, only five and four lines were observed in A_g and in B_g spectra, respectively, at 40 K. Three A_g lines at 628, 637 and 648 cm^{-1} originate from $2A_g$ (630 and 644 cm^{-1}) and B_{2g} (629 cm^{-1}) lines of phase I (the second B_{2g} component was not found in phase I [21]); the remaining two lines observed in this region at 620 and 667 cm^{-1} appear as a result of Brillouin zone folding and become visible below 200 K only. Two B_g lines at 630 and 638 cm^{-1} originate from zone-centre B_{1g} and B_{3g} modes whereas only two lines at 620 and 641 cm^{-1} were attributed as originating from the zone edge instead of four predicted. This fact apparently points to rather flat $\omega(k)$ dispersion curves of the corresponding phonon branches.

4.2. Internal modes of NH_4^+

The lowest-lying triply degenerate bending vibration ν_4^N (free ion value 1400 cm^{-1}) should have six A_g and six B_g lines. All the six components were unambiguously observed in A_g spectra at 40 K. Their pedigree is as follows: lines at 1420 and 1440 cm^{-1} come from B_{2g} modes, lines at 1403 and 1450 cm^{-1} from A_g modes of phase I, whereas the high-frequency

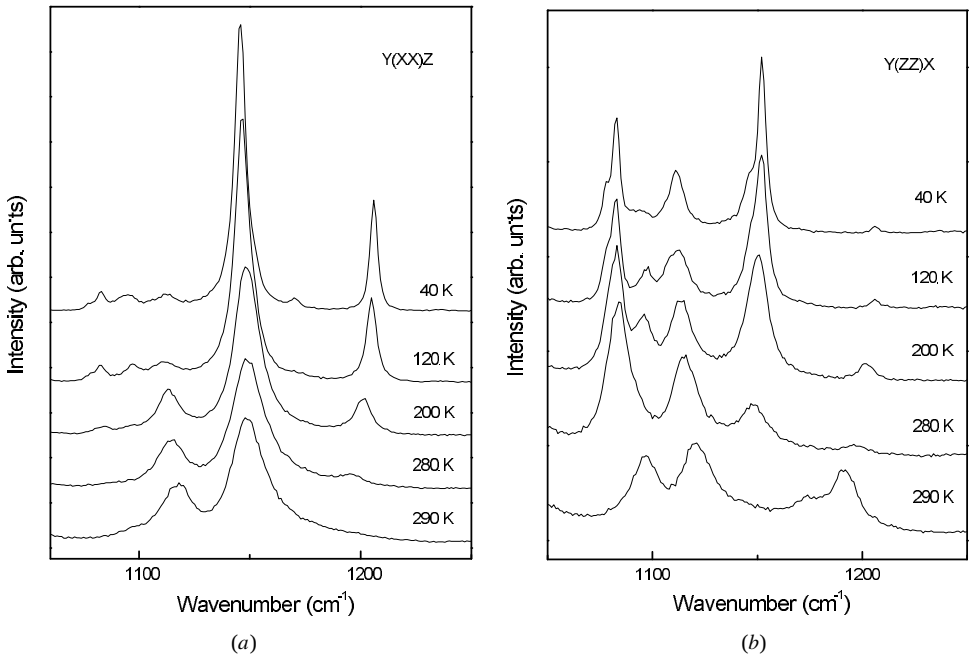

Figure 3. Temperature evolution of Raman spectra of LAS in the region of the ν_3^S stretching mode in $Y(XX)Z$ (*a*) and $Y(ZZ)X$ (*b*) scattering geometries.

lines of this group at 1473 and 1490 cm^{-1} originate from the X_2 zone-edge phonons. Among the B_g lines observed at 40 K in this region, lines at 1403 and 1418 cm^{-1} originate from B_{1g} and B_{3g} modes of phase I, respectively, while the others originate from the X_1 phonons.

In the region of doubly degenerate bending mode ν_2^N (free ion value 1680 cm^{-1}) four A_g and four B_g lines with equal frequencies in both species were observed in phase III in accordance with the correlation diagram. The low-frequency lines in this group, at 1686 and 1690 cm^{-1}, originate from A_g and B_{2g} modes of phase I, while the high-frequency lines at 1698 and 1702 cm^{-1} originate from zone edge phonons.

The region of the ν_1^N and ν_3^N stretching modes (free ion values 3040 and 3145 cm^{-1} respectively) is the most difficult to interpret because of Fermi resonance with overtones $2\nu_2^N$, $2\nu_4^N$ and $\nu_2^N + \nu_4^N$. Intense overtones and combinations observed in the vicinity of N–H stretching modes bring evidence for strong anharmonicity of ammonium ion vibrations in all phases. Very broad bands at 2850–2860 cm^{-1} were interpreted as $2\nu_4^N$ overtones in phase I [21] and have been also observed near 2860–2890 cm^{-1} at room temperature (phase II). On cooling down to 40 K these two-phonon bands split into six separate components lying between 2794 and 2940 cm^{-1}, their peak positions are in excellent agreement with the corresponding values of ν_4^N components (see table 2). The $2\nu_2^N$ overtones are undoubtedly seen at 3380 cm^{-1}, but only in A_g orientations, because ν_2^N lines are very weak in B_g spectra. Apparently, because of the Fermi resonance, the $\nu_2^N + \nu_4^N$ bands expected just in the region of ν_1^N and ν_3^N stretching modes greatly complicate Raman spectra. Moreover, due to the formation of H bonds, one can expect reconstruction in this spectral range. These circumstances lead to confusing results in detailed assignment of all components of fundamental modes. Nevertheless, it should be pointed out that formation of hydrogen bonding in phase III of LAS is corroborated by a downward shift of the ν_1^N and ν_3^N stretching frequencies and an upward shift of ν_2^N and ν_4^N bending frequencies.

Such shifts were not observed in phase I, giving evidence for considerably weaker or even broken H bonding at high temperatures. Similar effects have been also found in IR spectra of LAS [22] studied in all phases.

4.3. External modes

External vibrations of LAS extend up to 460 cm^{-1} and high-frequency Li^+ translations exhibit coupling with ν_2^S components. It is important to point out that most of the Raman lines predicted by factor-group analysis for phase III have been observed at the lowest temperature (40 K). Such an agreement happens rather rarely for a crystal containing as many as 88 atoms in the unit cell. Out of the 30 A_g and 30 B_g lines expected, all A_g and 24 B_g lines are listed in table 2. Temperature evolution of Raman spectra in the region of external vibrations is shown in figures 4 and 5.

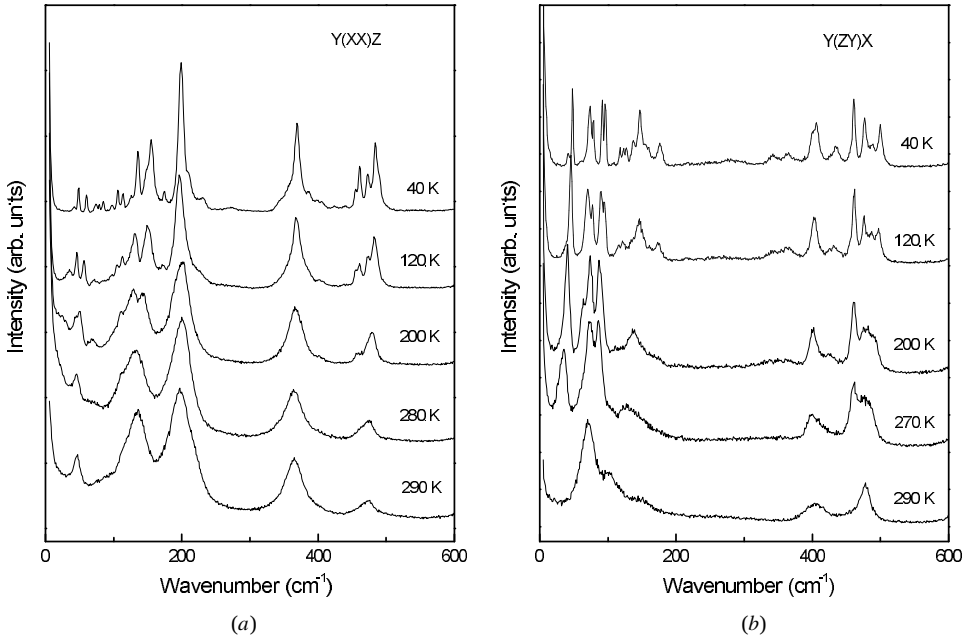

Figure 4. Temperature evolution of Raman spectra of LAS in the region of external modes in $Y(XX)Z$ (*a*) and $Y(ZY)X$ (*b*) scattering geometries.

The unit cell in phase III consists of two subcells where the structure of each subcell is similar to the ferroelectric one of phase II [6]. The atomic configurations in the upper half of the superlattice cell are those of the bottom half, mirrored by a plane perpendicular to the *y*-axis. Thus, the phase III structure can be seen as a periodically aligned micro-domain structure with alternating polarization [7]. In phase III, sulphate tetrahedra located in two neighbouring subcells are mutually rotated around the *a*-axis by an angle of about 46 degrees (at 213 K), whereas in phase II they are related by a simple translation. It is important to point out that no shifts of sulphur atoms were found at the II $\rightarrow$ III transition [6]. This structural transformation manifests itself in Raman spectra: namely, the spectra exhibit drastic changes in all non-diagonal orientations, while spectra in $Y(XX)Z$ orientation show gradual evolution at the II $\rightarrow$ III transition (compare figures 4(*a*) and 4(*b*)). Since external vibration frequencies exhibit considerable temperature dependence on cooling from T_2 down to 200 K one can

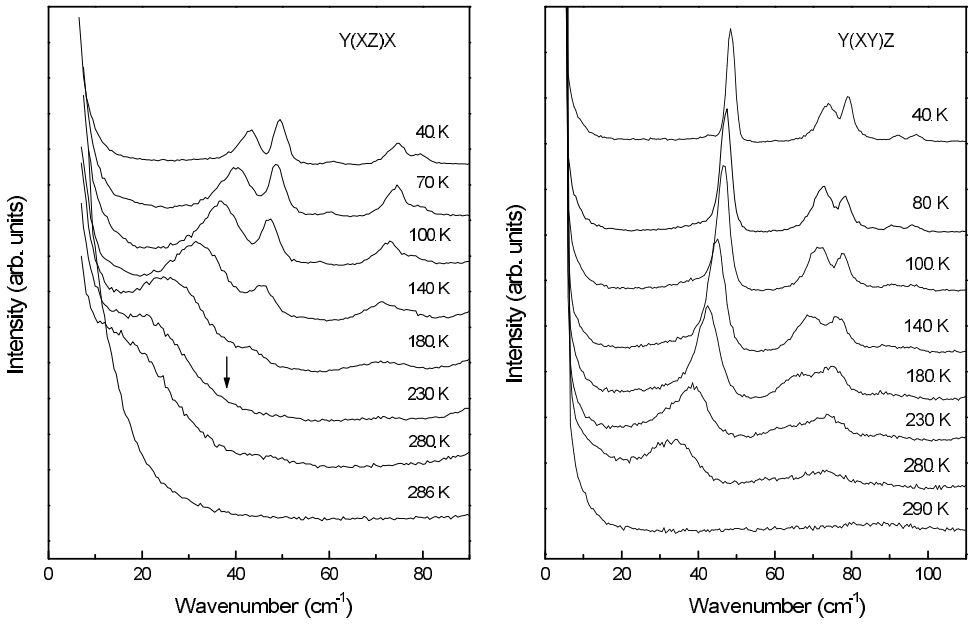

Figure 5. Temperature evolution of the low-frequency Raman spectra of LAS in $Y(XZ)X$ (*a*) and $Y(XY)Z$ (*b*) scattering geometries.

conclude that large-angle rotations of sulphate ions in phase III develop gradually and provoke hydrogen bond switching described above. No Raman lines have been found in phase II below 47 cm^{-1} whereas in phase III new lines at 24 and 36 cm^{-1} in A_g and B_g spectra, respectively, were observed just below T_2. In addition, on cooling, an additional line at 38 cm^{-1} was detected in A_g spectra (see the arrow in figure 5(*a*)). These lines arise apparently due to phonon branch folding at the transition. As follows from the correlations $X_1 \rightarrow A_u + B_g$ and $X_2 \rightarrow A_g + B_u$, the doubly degenerate soft mode splits in phase III into a Raman active A_g mode and an IR active B_u mode. The low-frequency A_g mode observed below T_2 may be attributed to the Raman component of the soft mode, while new lines at close frequencies of 36 cm^{-1} (B_g) and 38 cm^{-1} (A_g) are folded acoustic modes, $B_{1u} \rightarrow X_1$ and $B_{2u} \rightarrow X_2$, originating from transverse acoustic branches of phase I, which exhibit hard mode behaviour. The longitudinal branch $B_{3u} \rightarrow X_1$ apparently has twice the frequency of the transverse ones and presumably gives rise to one of the lines lying below 80 cm^{-1} where zone-centre or zone-folded optical phonons are also expected (see figure 5(*b*)).

As can be seen from figure 5(*a*) the Rayleigh line in $Y(XZ)X$ orientation was found to have approximately half the width in phase III of that in phase II. The lowest-lying A_g mode starts to appear as a shoulder of the Rayleigh line and exhibits significant temperature evolution on cooling. To obtain quantitative information the low-frequency Raman spectra were fitted with a sum of damped harmonic oscillators. For the purpose of the fit, the Rayleigh scattering wing at lowest frequencies was modelled by a fixed Lorentzian component with a halfwidth of about 4–5 cm^{-1} in the whole temperature interval. The resulting mode parameters obtained from the Raman spectra in the $Y(XZ)X$—A_g and $Y(XY)Z$—B_g geometries are presented in figure 6. Both folded acoustic modes show considerable narrowing on cooling from T_2 down to 130–140 K and the temperature dependences of their peak positions change slope in the same temperature interval. The soft mode is highly damped above 130 K where

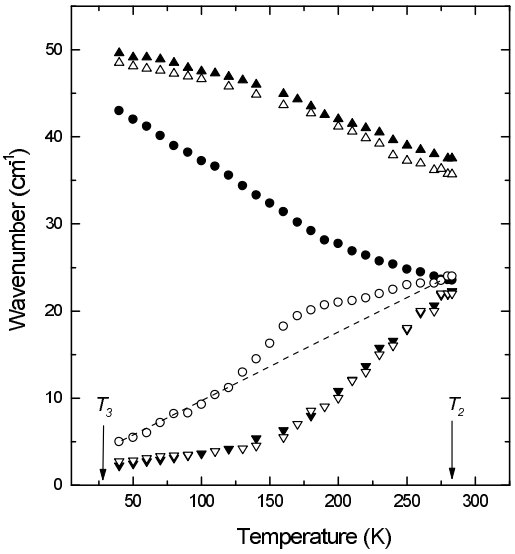

Figure 6. Temperature dependence of the parameters of the low-frequency modes of LAS shown in figure 5; full circles—frequency and open circles—halfwidth of the soft mode observed in $Y(XZ)X$ geometry; up triangles—frequency and down triangles—halfwidth of folded acoustic modes observed in $Y(XZ)X$ (full symbols) and $Y(XY)Z$ (open symbols) scattering geometries. The arrows mark the T_3 and T_2 phase transition temperatures.

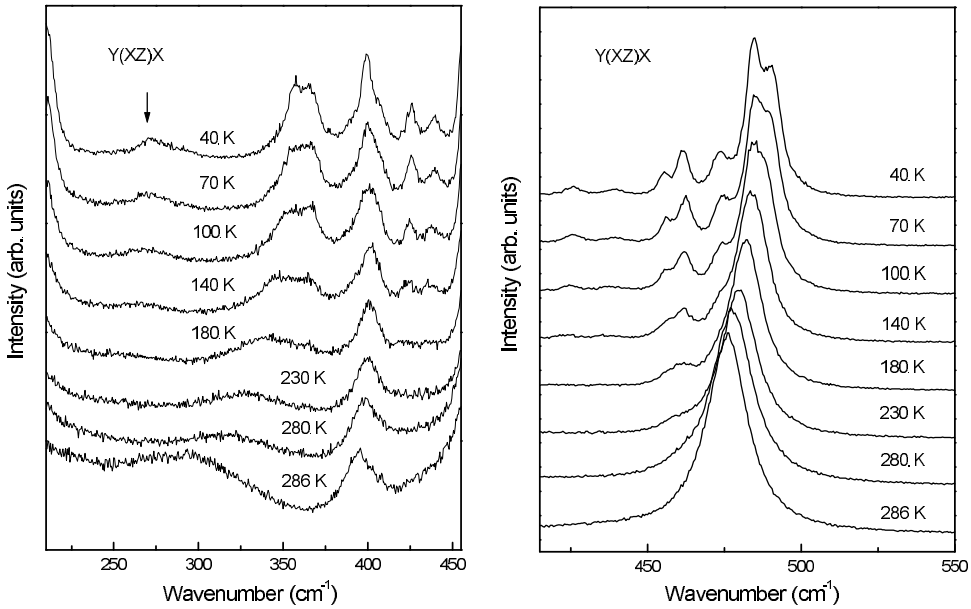

Figure 7. Temperature evolution of Raman spectra of LAS in the region of NH_4^+ librations and Li^+ translations (*a*) and (2S internal modes (*b*) observed in the Y(XZ)X scattering geometry.

its halfwidth increases considerably. This excess linewidth is apparently associated with heterophase fluctuations existing below T_2 down to 130 K.

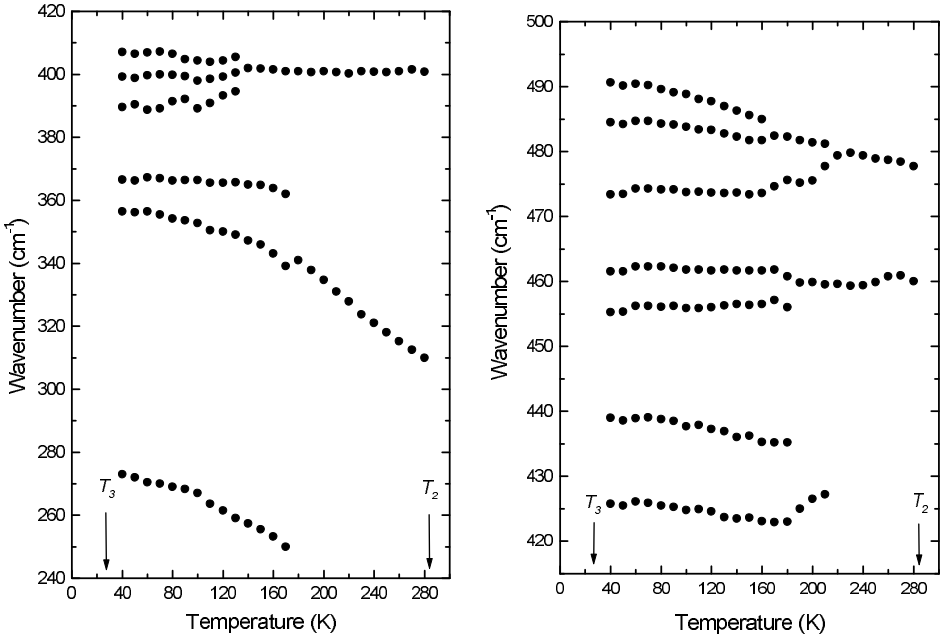

Figure 8. Temperature dependences of the frequencies of the decomposed Raman peaks shown in figures 7(*a*) and 7(*b*), respectively. The arrows mark the T_3 and T_2 phase transition temperatures.

Of interest is the behaviour of NH_4^+ librational modes and Li^+ translations lying in the region 250–460 cm^{-1}. As can be seen in figure 7(*a*), these lines exhibit a gradual narrowing on cooling and split into separate components far below T_2. We report here the temperature evolution in $Y(XZ)X$ orientation where both NH_4^+ librations and Li^+ translations are well presented and show typical temperature evolution. Applying the fitting procedure over the entire temperature interval, we found a temperature dependence of their frequencies presented in figure 8. We attribute the line at 393 cm^{-1} in phase II to Li^+ translations and the broad feature somewhat below 300 cm^{-1} (marked with an arrow in figure 7(*a*)) to NH_4^+ librations. The latter exhibits considerable hardening and narrowing on cooling below T_2 and splits into two lines below ∼200 K, one more line near 260 cm^{-1} emerging in the same temperature range. This is a strong indication that ammonium ions exhibit a gradual transition from large-amplitude reorientations to the small-amplitude ones, as that localization is necessary to obtain a well defined libration line. Temperature dependences of the halfwidths of NH_4^+ librational lines are presented in figure 9, where we plot the summed halfwidths for the lines at 356 and 366 cm^{-1} which merge into a single band above 200 K. As follows from these plots, all lines exhibit considerable narrowing on cooling and changes of slope of their linear dependence at 100 K. This feature allow us to assume that ammonium slowing down progresses rapidly below T_2 and is completed at a temperature of about 100 K. Given the absence of direct structural data below 190 K, we cannot prove our assumption conclusively. Nevertheless, this feature is in accord with PMR measurements [18, 19] where the presence of one threefold and two twofold simultaneous reorientations of ammonia in phase III was suggested. The changes in the reorientational frequency observed at 133 K and 81 K and interpreted as new PTs were, however, not confirmed by further investigations. It is important to point out that the significant increase of the proton second moment observed below ∼100 K [19] is direct

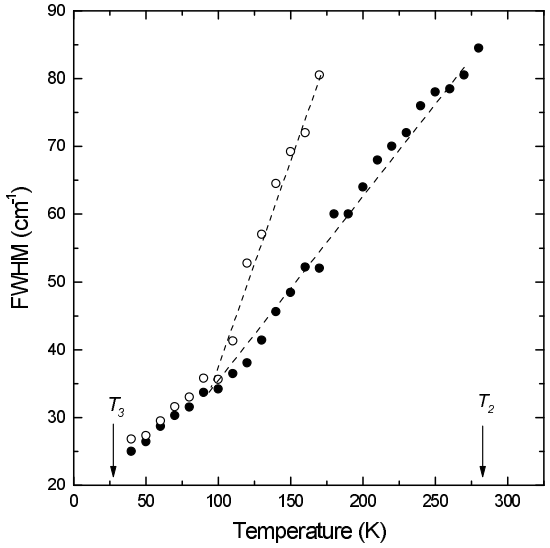

Figure 9. Temperature dependences of the halfwidths (FWHM) of NH_4^+ librations shown in figure 7(*a*); open symbols—the line at 273 cm^{-1}, full symbols—halfwidths of lines at 356 and 366 cm^{-1} (peak frequencies at 40 K) summed up. The arrows mark the T_3 and T_2 phase transition temperatures.

evidence of considerable slowing down of the motion of ammonium ions and is, in fact, in good agreement with our results.

The frequency of the Li^+ translational mode (399 cm^{-1} at 40 K) does not shows any variation in phase III apart from a drop down to 393 cm^{-1} at the III $\rightarrow$ II transition. As can be seen from figure 7(*a*), two satellites at 397 and 407 cm^{-1} become resolved below $\sim$130 K. The high-frequency Li^+ translational mode at 460 cm^{-1}, overlapping with the strong ν_2^S line at high temperatures, originates from a zone-centre A_g line observed in phase I and consists of two components which become resolved below 200 K. Finally, two weak lines originating apparently from zone-edge Li^+ translational phonons emerge at 425 and 439 cm^{-1} below $\sim$210 K. Four of the six A_g lines expected for Li^+ translations in phase III originate from zone centre modes of phase I and two come from zone edge ones. The latter were found unambiguously, while apart from lines at 455, 461 and 399 cm^{-1} originating from the zone centre phonons one of the satellites detected at lower temperature may be attributed to the fourth component. Since Li^+ mode frequencies display very weak temperature dependence in the whole range investigated, one can conclude that the Li–O distances do not vary from room temperature down to 40 K.

In contrast, as can be seen from figures 7(*b*) and 8(*b*), ν_2^S components exhibit gradual hardening on cooling; all three components observed in $Y(XZ)X$ orientation are apparently broad and overlapped above 200 K. Since ammonium reorientations modulate the potential of O atoms, the observed narrowing of ν_2^S components takes place simultaneously with the ammonium slowing down and hardening may be caused by the formation of hydrogen bonds.

5. Conclusions

Raman spectra of LAS exhibit significant temperature behaviour on cooling below T_2, indicating a considerable decrease in anharmonicity of ammonium and sulphate ions which

does not lead to any symmetry transformation down to 27 K. It is necessary to point out that most of the splittings expected due to the site symmetry lowering and unit cell doubling in phase III start to develop below ∼200 K and all components become resolved below ∼130 K or even below ∼100 K only, while at higher temperatures they are too weak or overlapped to be detected. Experimental Raman spectra of LAS are in good agreement with factor-group analysis far below T_2 and detailed assignments were performed at 40 K. The observed gradual changes in dynamics are apparently associated with large-amplitude reorientations of NH_4^+ ions which exhibit substantial slowing down on cooling, as revealed from the temperature evolution of Raman spectra and earlier PMR measurements [18, 19].

An unusual temperature dependence of the soft mode frequency and its halfwidth as well as gradual splitting observed in phase III is obviously caused by heterophase fluctuations which, in our case, extend far below T_2 and lead to numerous discrepancies in the interpretation of experimental results listed in the introduction. Summarizing the numerous experimental results one can conclude that a two-phase system in LAS exists in an extremely wide temperature range which may be divided into two intervals. The first one is the region where macroscopic, however metastable, regions of polar phase II exist below T_2 and induce piezo-and pyroelectric response and hysteresis loops. The disappearance of these macroscopic regions on cooling gives rise to anomalies in DSC and dielectric susceptibility measurements, which occur at different temperature values, depending on the cooling rate, size of the sample, thermal history, presence of electrodes, impurities etc. The process seems to be completed at 215 K where the pyroelectric response disappears [20] and no more anomalies in macroscopic properties of LAS below this temperature are reported. Raman spectra are considerably broader because of heterophase fluctuations in this temperature interval and, as demonstrated above, splittings expected in phase III start to develop below 200 K only, where the macroscopic regions of phase II vanishes. At lower temperatures the soft mode is still broad and considerable narrowing was observed below ∼160 K (see figure 6) where a weak anomaly of $\varepsilon(T)$ was detected [20]. This result obviously shows that heterophase fluctuations may exist even below 215 K and arise due to the presence of metastable polar clusters, which do not generate macroscopic polarization but lead to the increase of the linewidth. These clusters probably exist at least down to 133 K, where the formation of two antipolar subcells is completed due to slowing down of the ammonium ions evidenced from a slope discontinuity of the spin–lattice relaxation time in PMR measurements [18, 19] as well as from the temperature evolution of Raman spectra discussed above.

Acknowledgments

This work was supported by the Russian Foundation of Basic Research (project No 97-02-17878) and by the the Grant Agency of the Czech Republic (project No 202/98/1282) and the Grant Agency of the Academy of Sciences of the Czech Republic (project No A1010828). Critical reading of the manuscript by J Petzelt is gratefully acknowledged.

References

[1] Yuzvak V I, Zherebtsova L I, Shkuryaeva V B and Aleksandrova I P 1975 *Sov. Phys.–Crystallogr.* **19** 480
Yuzvak V I, Zherebtsova L I, Shkuryaeva V B and Aleksandrova I P 1978 *Sov. Phys.–Crystallogr.* **22** 182
[2] Mitsui T, Oka T, Shiroishi Y, Takashige M, Iio K and Sawada S 1975 *J. Phys. Soc. Japan* **39** 845
[3] Simonson T, Denoyer F and Moret R 1984 *J. Physique* **45** 1257
[4] Itoh K, Ishikura H and Nakamura E 1981 *Acta Crystallogr.* B **37** 664
[5] Dollase W A 1969 *Acta Crystallogr.* B **25** 2298
[6] Kruglik A I, Simonov M A and Aleksandrov K S 1978 *Kristallografiya* **23** 494

[7] Mashiyama H and Kasano H 1993 *J. Phys. Soc. Japan* **62** 155
[8] Torgashev V I, Dvorák V and Smutný F 1984 *Phys. Status Solidi* b **126** 459
[9] Kovalev O V 1965 *Irreducible Representations of the Space Groups* (New York: Gordon and Breach)
[10] Lemos V, Gomes P A P, Melo F E A, Mendes Fihlo J and Moreira J E 1989 *J. Raman Spectrosc.* **20** 155
[11] Torgashev V I, Yuzyuk Yu I, Smutný F and Polomska M 1986 *Sov. Phys.–Solid State* **28** 926
[12] Torgashev V I, Yuzyuk Yu I, Smutný F and Polomska M 1986 *Phys. Status Solidi* b **135** 93
[13] Abul Hossain M, Srivastava J P, Khulbe P K, Menon Lathika and Bist H D 1994 *J. Phys. Chem. Solids* **55** 85
[14] Lemos V, Centoducatte R, Melo F E A, Mendes Fihlo J, Moreira J E and Martins A R M 1988 *Phys. Rev.* B **37** 2262
[15] Poulet H and Mathieu J P 1977 *Solid State Commun.* **21** 421
[16] Chhor K, Abello L and Pommier C 1989 *J. Phys. Chem. Solids* **50** 423
[17] Smutný F and Polomska M 1988 *Ferroelectrics* **79** 209
[18] Watton A, Reynhardt E C and Petch H E 1978 *J. Chem. Phys.* **69** 1263
[19] Reynhardt E C, Watton A and Petch H E 1982 *J. Chem. Phys.* **76** 5761
[20] Gerbaux X, Mangin J, Hadni A, Perrin D and Tran C D 1982 *Ferroelectrics* **40** 53
[21] Torgashev V I, Yuzyuk Yu I, Smutný F and Polomska M 1988 *Kristallografiya* **33** 1181
[22] Alam S and Srivastava J P 1981 *Spectrochim. Acta* A **37** 183
[23] Smutný F and Polomska M 1984 *Phys. Status Solidi* a **82** K33